UDC 531.32:519.876.5
DOI: 10.15587/2706-5448.2024.310428

Abdelghani Khellaf,
Mouloud Mansouri

DEVELOPMENT OF THE STICK-SLIP FRICTION MODEL FOR DISCRETE ELEMENTS MODELING

The object of the research is an intergranular friction model for use in discrete-element modeling of the mechanical behavior of granular materials under static and dynamic conditions. As in this approach grains are modeled by independent elements interacting through contact forces, the selection of contact force models, and in particular for the tangential component (friction), represents the most important task in obtaining the most realistic macroscopic behavior. There are many friction models that work well in dynamic regimes, but fail to model mechanical behavior in static or quasi-static regimes. In this work, an intergranular friction model is proposed based on Coulomb's regularized friction model, which takes into account the stick-slip phenomenon that appears at low sliding speeds at the contact. Three different examples are designed and modeled in order to demonstrate the robustness of the model in different situations including static, quasi-static and dynamic regimes. The first is a basic example consisting of the translational motion of a grain on a planar surface with a relatively low constant velocity. This example allowed to capture the stick-slip phenomenon. The second represents a grain subjected to its own weight and supported essentially by frictional forces. This example shows that the model works well in both quasi-static and static regimes. The third example consists of a grain sliding on a plate and subjected to accelerated motion. It showed the effect of friction velocity on the occurrence of stick-slip, as well as the evolution of friction force with sliding velocity. The obtained results demonstrated that the model effectively captures shear behavior in the different regimes. It could therefore be used in discrete element modeling of granular materials under both static and dynamic conditions. As in this work, the model is formulated in 2D, it would be interesting to develop a general 3D formulation so that it can be easily applied in 3D modeling.

Keywords: *Coulomb friction, static, dynamic, stick-slip, discrete element method, soft contact, shear rate.*

Received date: 07.06.2024
Accepted date: 23.08.2024
Published date: 26.08.2024

How to cite
Khellaf, A., Mansouri, M. (2024). Development of the stick-slip friction model for discrete elements modeling. Technology Audit and Production Reserves, 4 (1 (78)), 17–25. https://doi.org/10.15587/2706-5448.2024.310428

1. Introduction

The discrete element method (DEM) is a numerical technique used to simulate the behavior of granular materials by modeling each particle as a discrete entity with its own position, velocity, and contact forces. For the intergranular contact treatment two distinct methodologies can be distinguished. the soft-contact approach [1] and the hard-contact approach [2, 3]. In the soft-contact approach firstly invented by Cundall and Strack, 1979, the particles are modeled as pseudo-rigid bodies with deformation mainly occurring at the contact point, allowing a small particle deformation referred as overlap. This latter is then used to calculate the contact forces modeled via rheological models selected to reproduce the overall behavior of granular media in a given context [4–7].

In the soft-contact modeling of dry granular media, the intergranular forces are commonly decomposed on normal and tangential forces. This latter is governed by intergranular friction which has a determinant effect on the macroscopic behavior of the simulated material [8–10]. Therefore, the development and calibration of friction models in DEM are essential to ensuring the fidelity and effectiveness of simulations in studying granular systems and complex particle interactions. In this context, many friction models are developed, some of these models are based on Coulomb friction laws [1, 11–13] and others on elastic Mindlin's theory [14–16].

The aim of this research is to present the dry friction model extended to the stick-slip behavior commonly observed in systems characterized by friction coefficients different in static and dynamic regimes. First, the model is formulated and implemented in a 2D discrete element model. Then, three examples involving a static, quasi-static and dynamic situations are modeled and analyzed in detail to show the effectiveness and robustness of the model.

2. Materials and Methods

2.1. Stick-slip motion. When two surfaces are in contact, they are effectively in contact only in certain areas, called asperities [17, 18], Fig. 1, 2. The junctions created by the contacts at the level of the asperities have two behaviors during shearing motion.

Stick stage: Under the effect of an external force of small amplitude, the links stretch and allow a microscopic relative displacement between the two surfaces in contact. This deformation is «reversible», therefore, if the external force cancels, the deformation disappears, the two solids resume their relative starting position.

ISSN 2664-9969

Slip stage: Under the effect of external force of amplitude greater than coulomb's threshold $\mu_s F_n$, called the «breakaway force», the deformation is irreversible, the connection created by the asperities break and relative sliding occurs.

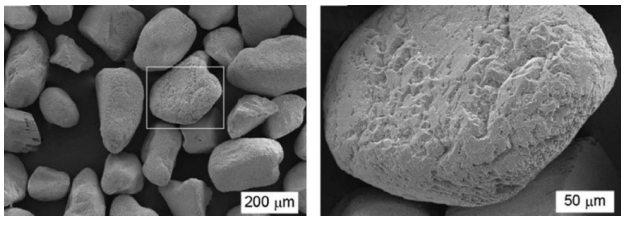

a *b*

Fig. 1. Ottawa sands: *a* – SEM photomicrograph, *b* – an enlargement image of the framed area in (*a*) [19]

Stick-slip motion is characterized by a sawtooth displacement-time evolution. Fig. 3 illustrates the static phase and the kinetic phases involving the stick-slip phenomenon. The motion is bonded by the static friction force $\mu_s F_n$ in the stick phase and the kinetic friction force $\mu_k F_n$ in the slip phase. Where μ_s and μ_k are respectively the static and the dynamic friction coefficients with $\mu_k < \mu_s$.

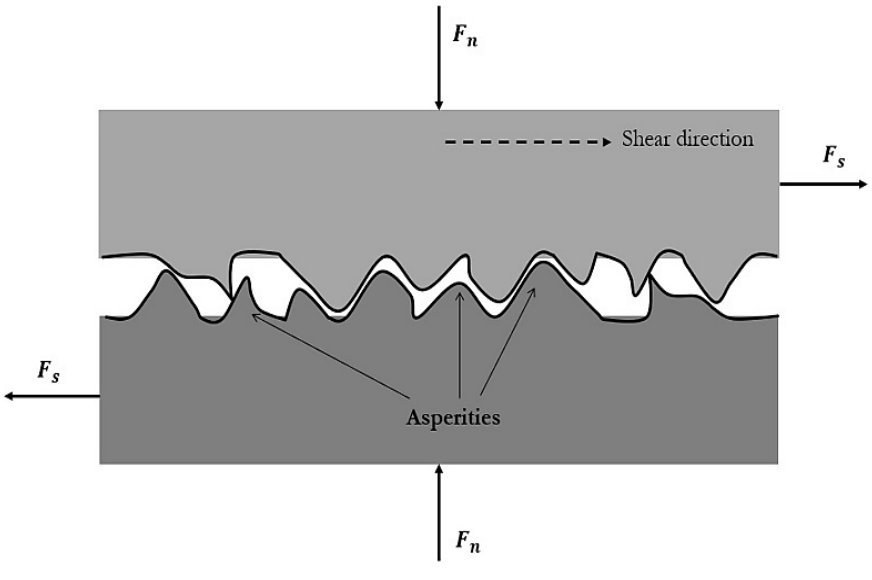

Fig. 2. Schematic view of the microscopic contact of tow surfaces: F_n – normal forces, F_s – shear forces

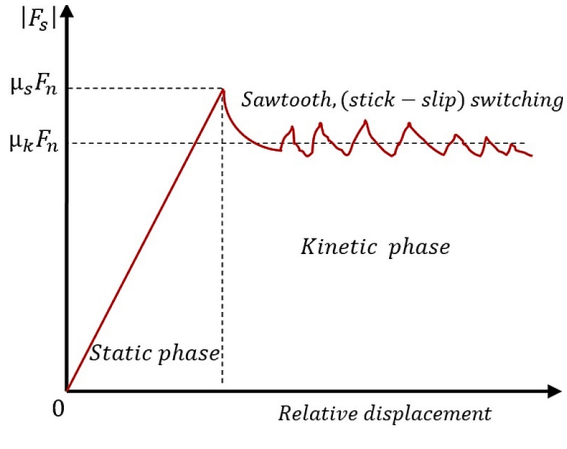

Fig. 3. Illustrative scheme of stick-slip behavior

A number of factors affect the stick-slip phenomenon. The most important factors are: the shear velocity and the quantity and nature of asperities of the contact surface. The shear velocity V_S has a very important effect on the frictional force. The experiments show that the average friction force F_s depends on the shear rate. Typically, F_s decreases as V_S increases as shown in Fig. 4.

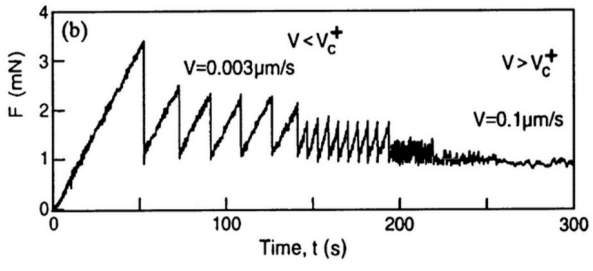

Fig. 4. Typical evolution of friction force in terms of shear velocity V_c^+ being the critical shear velocity [20]

The critical shear velocity V_s^c is defined as the velocity beyond which the friction force disturbances due to stick-slip become negligible, above this velocity the relative surfaces motion is referred to as steady sliding [20–24].

2.2. Usual contact models in DEM.

In 2D simulation of granular media composed of circular-shaped particles, each grain i is defined by its mass m_i, radius r_i and position $\vec{x}_i$ and the same for grain j, the deformation of the grains is parametrized by the overlap $D_n = (\vec{x}_i + \vec{x}_j) - (r_i - r_j)\vec{n}$ (Fig. 5). The dynamics of a grain i is governed by second Newton's law, where the equations of translation and rotation are integrated involving all external forces acting on this grain such as contact forces and gravity:

$$m_i \ddot{\vec{x}}_i = \overrightarrow{F_{ij}^C} + m_i \vec{g}. \quad (1)$$

The contact force $\overrightarrow{F_{ij}^C}$ defined as the action of the grain j on the grain i can be decomposed into normal and tangential components, $\vec{F}_n$ and $\vec{F}_s$ respectively:

$$\overrightarrow{F_{ij}^C} = F_n \vec{n} + F_s \vec{s}, \quad (2)$$

where $\vec{n}$ is the normal unit vector pointed from i to j, and $\vec{s}$ is the tangential unit vector obtained from a+90° rotation of $\vec{n}$.

For the normal component, particles collusion is commonly modeled with linear visco-elastic model. Where the contacting grains are treated as a harmonic damped oscillator having an effective masse equals to $m_i m_j / (m_i + m_j)$. The natural half-period of this oscillator is considered as the contact duration T_C. This latter is discretized into small time steps dt in order to properly resolve the contact evolution.

Thus, $\overrightarrow{F_n}$ is the sum of the elastic and damping forces:

$$\vec{F}_n = (D_n K_n + v_n V_n)\vec{n}, \quad (3)$$

where K_n is the normal stiffness of the spring and V_n is the velocity of grain i relative to grain j velocity given by:

$$V_n = \left(\vec{x}_j - \vec{x}_i\right)\vec{n}, \quad (4)$$

more details about normal force modeling are presented in references [6, 7, 16, 25, 26].

The tangential component $\overline{F_s}$ is often represented by models based on Coulomb's law, due to their simplicity of implementation and short computational time. For dynamic problems, the linear model is the most representative. This model assumes that the frictional force is proportional to the normal contact force according to Coulomb's law. the disadvantage of this model is that the tangential force becomes undefined if the interparticle shear velocity is zero ($\overline{V_s} = \vec{0}$). For static or quasi-static problems tow models was distinguished. The visco-plastic model and visco-elastic friction model in both the tangential force was limited by coulomb threshold, beyond this threshold an intergranular slip occurs. These models are summarized in Table 1.

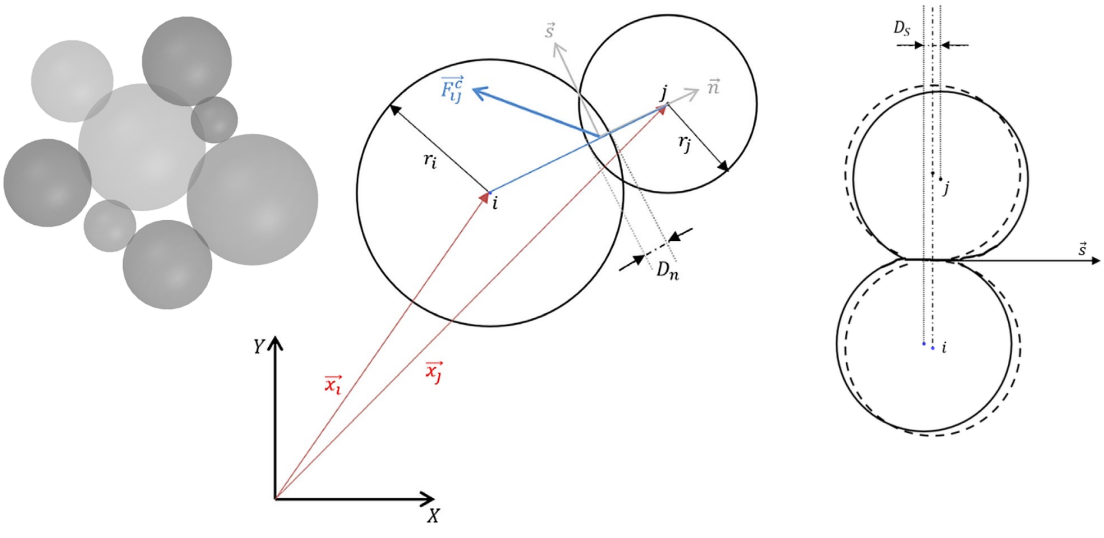

Fig. 5. Soft-contact particles interaction

Table 1

Usual friction model

Rheologic model	Description	References
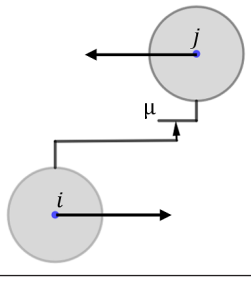	Coulomb friction model: $\vec{F}_s = \mu\lvert F_n\rvert sign\left(\overline{V_s}\right)$, $\mu = \mu_k$, where $\vec{V}_s$ – relative shear velocity	[27–29]
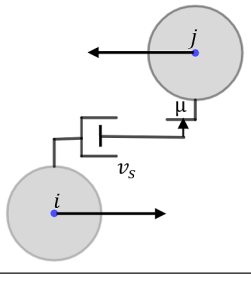	Visco-plastic model: $\vec{F}_s = \min\left(\lvert v_s V_s\rvert; \lvert\mu F_n\rvert\right) sign\left(\overline{V_s}\right)$, $\mu = \mu_k$	[26, 30, 31]
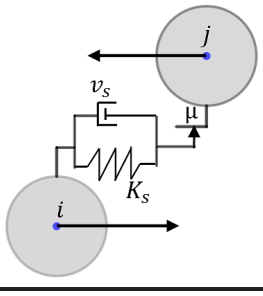	Visco-elastic model: $\vec{F}_s = \min\left(\lvert K_s D_s + v_s V_s\rvert; \mu\lvert F_n\rvert\right)$, $sign\left(K_s D_s + v_s V_s\right)$, where v_s – damping coefficient	[12, 13, 32–34]

ISSN 2664-9969

2.3. Stick-slip friction model. In this section, the tangential contact model and the calculation algorithm during a contact evolution will be presented in detail. The tangential force is modeled by an elastic spring with a dashpot in series with a slider (Fig. 6). The elastic spring allows to simulate the deformation or the reversible phase (*stick phase*) and the slider defines the Coulomb's threshold characterized by different friction coefficients in static and dynamic regimes.

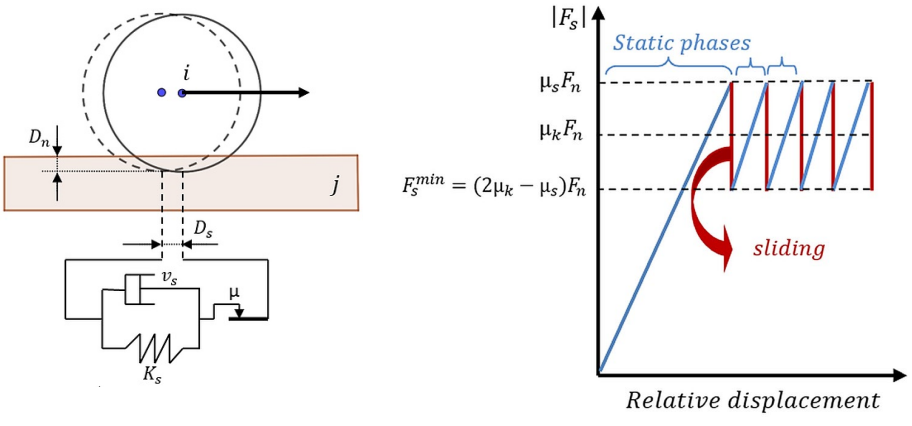

Fig. 6. Stick-slip friction model

As mentioned in subsection 2.1, stick-slip motion has static and dynamic phases. In the static phase the stick force remains below the coulomb's static threshold $F_s \le \mu_s F_n$ and the spring deformation is equal to the relative tangential displacement D_s. Therefore, the tangential force is computed as the sum of the elastic force and the viscous force:

$$\vec{F}_s = \left(-D_s K_s - v_s V_s\right)\vec{s}, \qquad (5)$$

where K_s is the tangential spring stiffness and V_s the relative tangential velocity:

$$\vec{V}_s = (V_j - V_i)\vec{s}. \qquad (6)$$

During contact evolution D_s increases at each time step (dt) so that:

$$D_s = \sum_{dt} V_s dt. \qquad (7)$$

Once the tangential force exceeds the Coulomb's static threshold $F_s \ge \mu_s F_n$ the kinetic phase is activated and F_s set to $F_s^{\min}$. In this moment the spring deformation should be adjusted to conform the kinematic friction force:

$$D_s = \frac{F_s^{\min}}{K_s}. \qquad (8)$$

Immediately another stick phase will be activated. It should be noted that the lower limit of the friction force $F_s^{\min}$ during the stick-slip motion is chosen $(2\mu_k - \mu_s)F_n$ so that the average tangential force is equal to $\mu_k F_n$.

The model implementation can be done according to the diagram in Fig. 7. This diagram indicates that calculation of the shear force begins from the moment contact begins, i. e. ($D_n < 0$). At this moment, contact duration and shear deformation are initiated to zero ($t = 0$ and $D_s = 0$). During the contact, the algorithm checks if the stick force is less than the static threshold; if so, it calculates the static friction force using the tangential deformation and maintains the state as «sticking».

When the stick force exceeds the static coulomb's threshold, the algorithm transits to the slipping phase, where it calculates the friction force using the dynamic friction coefficient, the friction force drops below the dynamic threshold again, the system returns to the sticking phase. This process is repeated for as long as the contact continues. The Coulomb slip threshold evolves with time, since it depends on the normal contact force, which varies with time.

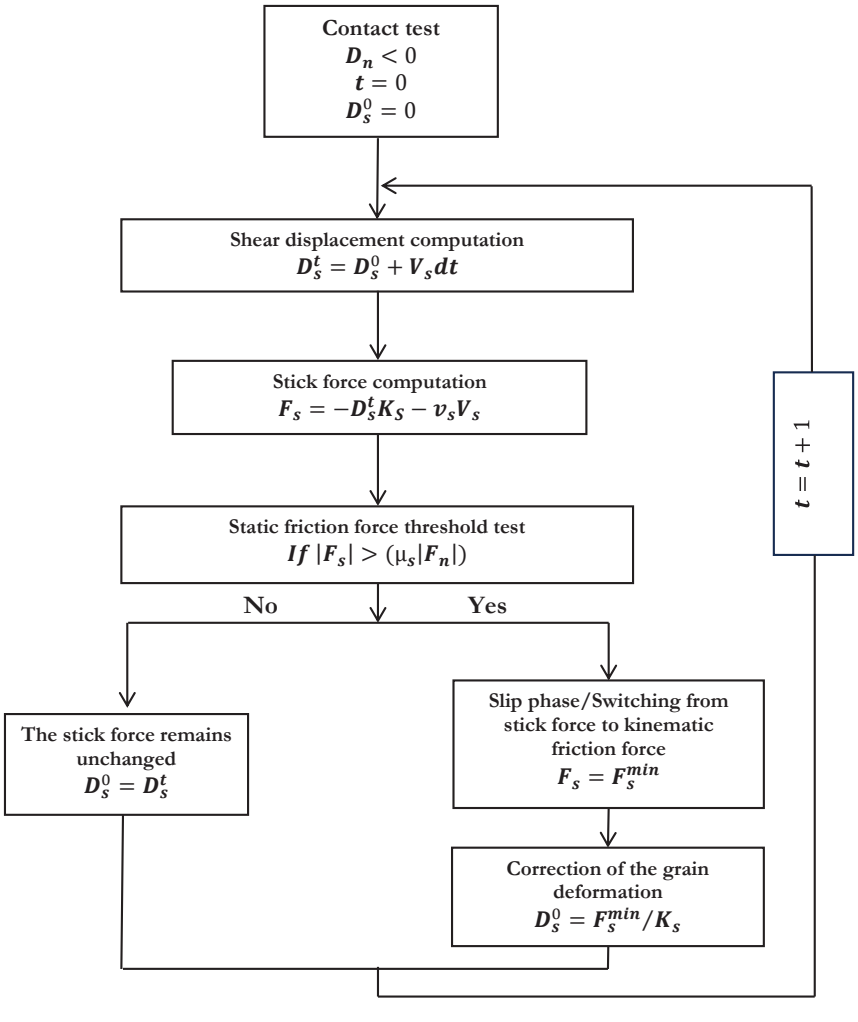

Fig. 7. The diagram of the model implementation

3. Results and Discussion

It should be mentioned that, in the following examples, the grains motion is assumed to be a pure translation without rolling, so that the sliding velocity equals to the translational velocity. These examples allow to highlight the friction force evolution.

The common parameters for all simulations are summarized in Table 2.

Table 2

Simulations parameters

Characteristics	Symbol	Value	Unite
Normal stiffness	K_n	12000000	N/m^2
Tangential stiffness	K_s	9600000	N/m^2
Normal viscous damping coefficient	v_n	41.38	kg/s^{-1}
Tangential viscous damping coefficient	v_s	33.10	kg/s^{-1}
Static friction coefficient	μ_s	0.5	–
Kinetic friction coefficient	μ_k	0.45	–
Gravity	g	9.81	m/s^2
Density of grains	ρ	2600	kg/m^3

3.1. Quasi-static example. A basic example which shows the stick-slip phenomenon consists on a grain translation on a planar surface (Fig. 8), the grain i has a radius $r = 0.002$ m and mass m_i, it is supported by a planar surface and subjected to a constant horizontal velocity ($V = 0.00001$ m/s), this velocity is selected relatively small in order to observe the stick-slip phenomenon.

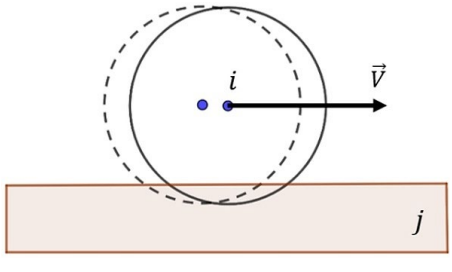

Fig. 8. Circular shaped grain translating on a planar surface

The friction force and the grain's slippage evolution as function of the relative displacement between the grain and the planar surface are shown in Fig. 9. For the friction force plot, two main phases are distinguished, a static phase and dynamic phase. In the first one, the relative displacement equals to the grain deformation without sliding. In this case, the friction force increases linearly until reaching the coulomb's static threshold $\mu_s F_n$. In the dynamic phase, the stick-slip phenomenon occurs where the frictional force switches between the static limit $\mu_s F_n$ and the dynamic limit $(2\mu_k - \mu_s)F_n$. During the sticking periods, the frictional force increases linearly to reach the static friction limit, as described in phase 1. However, when F_s reaches the static frictional limit, the grain starts to slip and the frictional force drops to the dynamic friction limit. This drop in frictional force is represented by a vertical line segment in the graph.

As mentioned in the description of the model, the lower limit of the friction force $F_s^{\min}$ during the stick-slip motion is chosen so that the average tangential force is equal to $\mu_k F_n$.

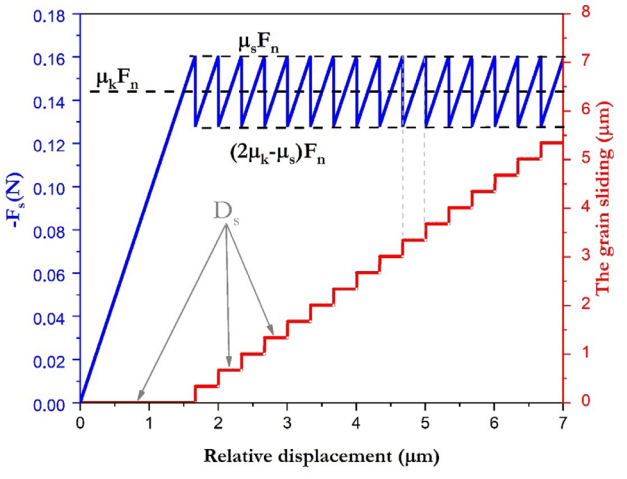

Fig. 9. The friction force and the grain sliding evolution

During translation, it is noticed that the grain makes sliding jumps presented on the graph by vertical segments (slip segments), and deformation phases presented by horizontal segments (stick segments). during the stick phase there is no sliding between the grain and the planar surface and the friction force increases linearly as the deformation increases.

3.2. Static example. In order to highlight the differences between the friction models presented in subsection 2.2, a simple static problem is simulated. In this problem, two circular particles denoted 1 and 2, with equal radii $r_1 = r_2 = 0.005$ m and masses $m_1 = m_2$, are placed in a rectangular tray (Fig. 10). The length L of the tray is less than the sum of the diameters of the two grains $L < (2r_1 + 2r_2)$. In addition, since the grains are slightly deformable, L is selected sufficiently large so that the normal forces alone cannot support the weight of grain 1.

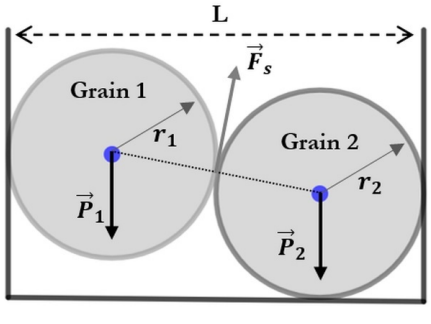

Fig. 10. Schematic illustration of the static example

Initially, the grains are placed almost in contact. At the instant $t = 0$, the acceleration of gravity is applied to the system, therefore, the grain 1 moves downwards and the contact forces between the grains develop.

The evolution of the vertical position of the grain 1 for different friction models is shown in Fig. 11.

It can be observed that both models (coulomb model and the visco-plastic model) exhibit a nonrealistic behavior, in fact the grain 1 can't be supported by the friction forces and reaches at the end the bottom of the tray. Let's note that the grain displacement has different paths for these two models. Contrarily, for the viscoelastic model with stick-slip, shows a more realistic behavior where the grain 1 is supported by the contact forces in a position above the bottom of the tray.

ISSN 2664-9969

In order to understand the observed behaviors, the evolution of the grain-grain tangential force with time is plotted in Fig. 12 for the three models.

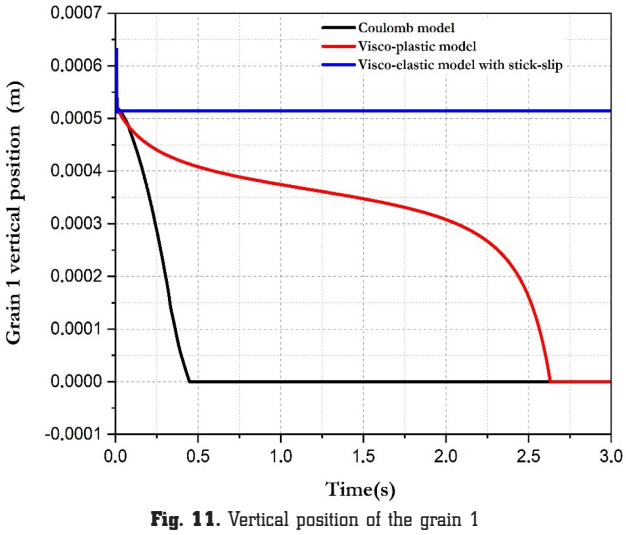

Fig. 11. Vertical position of the grain 1

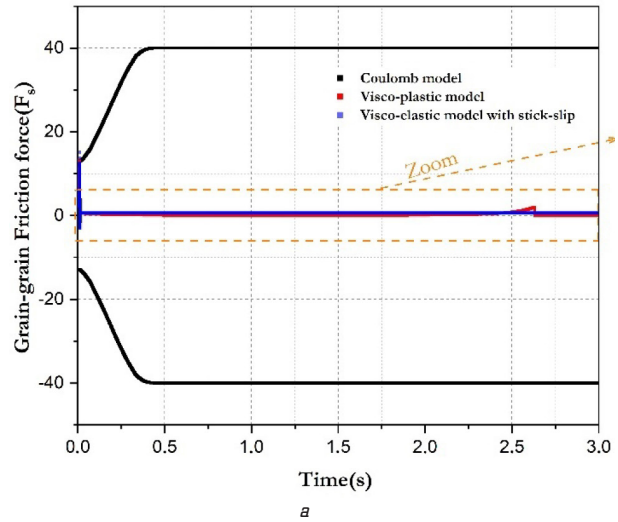

a

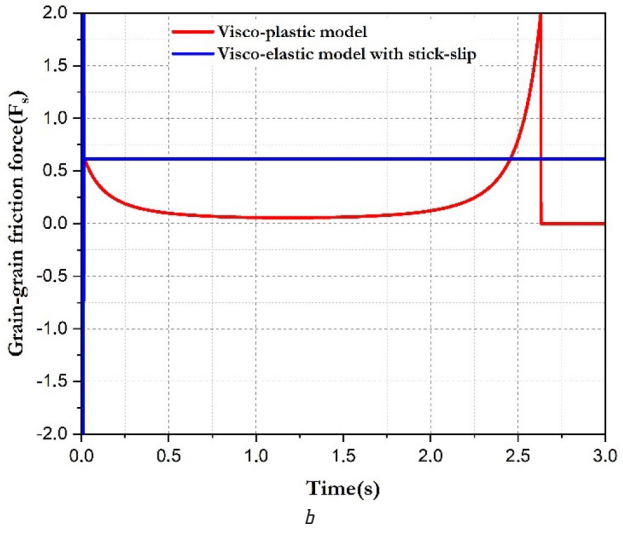

b

Fig. 12. Comparison between the presented friction models: *a* – coulomb model; *b* – visco-plastic model

Fig. 12, *a* shows that, for the Coulomb model the tangential force alternates between two equal values of different signs. Since the average of these values is zero, the grain 1 cannot remain suspended above the bottom of the tray. It should be noted that the friction force values correspond to the static Coulomb's threshold that evolves with the grain displacement which induces the increase in the overlap and consequently the increase in the normal force. Compared to the Coulomb's model the friction force values for the other models are very small. These forces result from the tangential deformation of the grains.

For the visco-plastic model (Fig. 12, *b*), at the beginning of the test, the grain 1 reaches a certain vertical velocity before the initiation of the contact, which is why the friction force is initially close to 0.6 N. This latter gradually slows down the grain 1 which decreases the relative tangential velocity to reach a zero value. Consequently, the friction force becomes close to zero and the grain restarts an accelerated downward movement under the effect of its weight. The increase in the velocity produces an increase in the friction force until the instant t=2.65 s, where the grain reaches the bottom of the tray (Fig. 11). Thus, from this moment the velocity of the grain 1 becomes zero. It can be concluded that at a quasi-static regime, the visco-plastic model alternates the movement between accelerated and decelerated, which leads to a continuous movement of the grain.

For the visco-elastic model with stick-slip, the friction force reaches a constant value (close to 0.6 N) from the beginning of the test. This allows to retain the grain 1 locked between the gain 2 and the tray wall under the effect of this force as well as the normal contact force.

3.3. Dynamic example. The aim of this example is to show the transition from static to dynamic regime and the effect of the translation velocity on the friction force modeled through the visco-elastic with stick-slip model. In this simulation a particle of weight $\vec{P}$ placed on a non-deformable plate initially horizontal. This plate is then rotated with a constant angular velocity until reaching the coulomb static threshold, i. e. $\tan\beta=\mu_s$ (β – plate inclination). It should be noted that the grain motion is due to its own weight and the grain rotation is locked such that it undergoes only a translation motion as illustrated in Fig. 13. In this way the shape of the grain (circular, rectangular, square, etc.) has no effect on the results, the circular element is chosen, since it is the most common element used in DEM modeling practice.

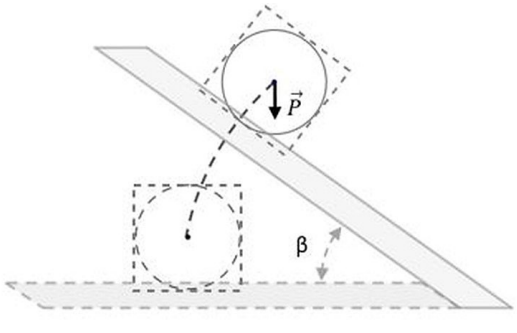

Fig. 13. Schematic representation of the performed test the grain can undergo only a translation motion, the rotation being locked

Fig. 14, *a* shows the evolution of the surface inclination angle β and the friction force with time. It is clear that before the motion triggering $\tan\beta\leq\mu_s$, β evolves linearly with time since the rotation velocity of the plate is constant. Whereas, the evolution of the friction force follows

the sinusoidal form $\sin\beta$ given that it is the reaction to the tangential driving force which is equal to $\bar{p}\sin\beta$. When $\tan\beta = \mu_s$, F_s reaches the static threshold and the grain starts to slid.

Fig. 14, *b* shows a zoom of the dynamic part of the test where β is maintained constant such as $\tan\beta = \mu_s$. In this case the friction force evolution could be decomposed in three distinct phases: a transition phase, a stick-slip phase, and a steady sliding phase. The transition phase represents the transition from the static equilibrium state to the sliding state. It is notable that, when the rotation of the plate stops, the grain momentum causes a sharply and instantaneous decreasing in the normal force, which causes a sharply decreasing in the friction force. The variation in the tangential force in this phase is due to the variation in the normal force caused by the normal movement of the grain resulting from the sudden stop of the plate.

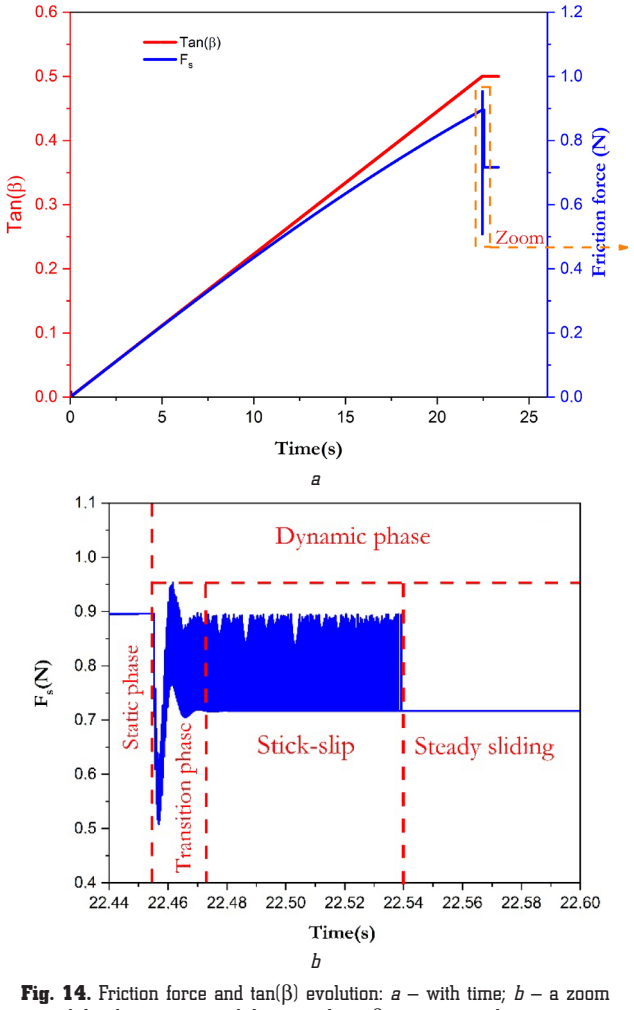

Fig. 14. Friction force and tan(β) evolution: *a* – with time; *b* – a zoom of the dynamic part of the test where β is maintained constant such as $\tan\beta = \mu_s$

After the transition phase, the grain enters the stick-slip motion and the friction force switches between static and dynamic thresholds as described in example 1. During this phase the average of the friction forces is lower than the static limit, the balance of forces produces a non-zero acceleration, consequently the movement of the grain becomes accelerated. At the beginning of the stick-slip phase, the grain has a low translation velocity and the stick stage is well resolved as illustrated in Fig. 15. Therefore, the average of the friction forces is close to $\mu_k F_n$. With the increase in the translation velocity the stick stage becomes poorly resolved and sometimes undetectable, therefore, the slip stage becomes predominant and the average of the friction forces decreases. As a result, during this phase the friction forces average is decreasing thus the movement acceleration is continuously increasing as shown in Fig. 15.

When the translation velocity is sufficiently high, the stick stages become invisible, the friction force is constant and equals to $F_s^{\min}$, thus the acceleration remains constant (Fig. 15). This is the steady sliding phase, where continuous and smooth motion occurs.

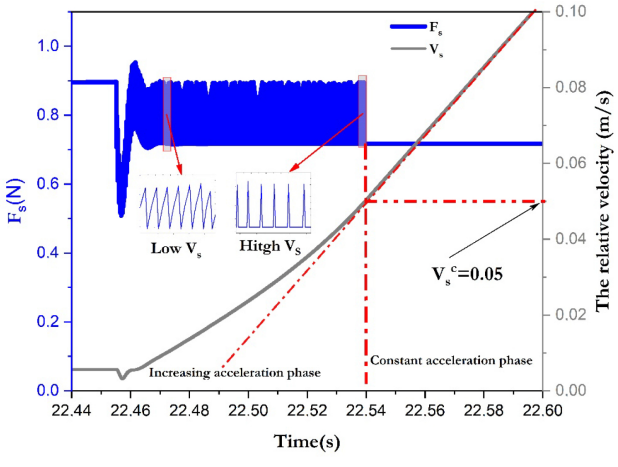

Fig. 15. Translation velocity evolution

The above behavior is generally in good agreement with what has been observed experimentally as described in Fig. 4. Therefore, the friction model presented in this paper captures clearly the effect of the shear rate on the friction force. This latter will be detailed in future research and more parameters should be studied.

3.4. Discussion of results and model. A two-dimensional model of friction that incorporates the stick-slip phenomenon offers valuable insights into the complex interactions between surfaces in contact. In the presented model, the stick-slip behavior is characterized by phases of static friction (stick) followed by sudden motion (slip). These phases are governed by the elastic deformation, the static and dynamic Coulomb friction coefficients. In this research work, numerical tests with details on the evolution of the tangential force with displacement (stick and slip) were carried out. These tests have shown that the model effectively captures the characteristics of static and dynamic intergranular friction. In particular, these tests have shown that formulating the model in the way presented here captures the dependence of friction force on tangential velocity in the case of dynamic sliding, a phenomenon well known from experience. This model could thus contribute, through discrete element modeling, to the understanding of phenomena involved in the mechanics of granular materials. It should be remembered, however, that the precision of numerical modeling results, always depends on the introduced model parameters. For this model, the micromechanical input parameters, i. e. the tangential elastic stiffness and the static and dynamic friction coefficients, should be well identified in order to achieve efficient modeling.

Besides, in this work, the model is presented in 2D configuration, in which only one deformation variable per contact is required. When considering the extension of this model to 3D discrete element modeling, certain difficulties arise: firstly, the number of contacts increases rapidly with the number of grains; secondly, shear deformation is characterized by three variables per contact. This leads to substantial increases in computational time and memory requirements. The challenge, therefore, is to achieve a simplified 3D formulation of the model that can be less memory- and computation-time-consuming, and this is one of the aims of future work.

4. Conclusions

Discrete element modeling is a powerful tool for simulating the different phenomena and behaviors related to the granular materials. The micro-macro relationship is governed by the appropriate choice of rheological models at the intergranular contact's level. In this work a dry friction model for DEM soft contact modeling is formulated and analyzed. The model is based on the regularized Coulomb friction model accounting for the stick-slip behavior. Various numerical validation tests have been designed and carried out, the first test explored the quasi-static regime, in which it is shown that the model successfully depicts the alternating periods of sticking and slipping. The second example focused on the static regime, where it is demonstrated that the model operates robustly for zero shear rate cases. Such a performance is crucial for applications where objects remain stationary and are subjected to gradually increasing forces. The third example combined both static and dynamic regimes. Through this example, it is shown that the model effectively captures the variation of the friction force with the shear rate.

Conflict of interest

The authors declare that they have no conflict of interest concerning this research, whether financial, personal, authorship or otherwise, that could affect the study and its results presented in this paper.

Financing

The study was performed without financial support.

Data availability

The paper has no associated data.

Use of artificial intelligence

The author confirms that he did not use artificial intelligence technologies when creating the presented work.

References

1. Cundall, P. A., Strack, O. D. L. (1979). A discrete numerical model for granular assemblies. *Géotechnique, 29 (1),* 47–65. https://doi.org/10.1680/geot.1979.29.1.47
2. Hong, D. C., McLennan, J. A. (1992). Molecular dynamics simulations of hard sphere granular particles. *Physica A: Statistical Mechanics and Its Applications, 187 (1-2),* 159–171. https://doi.org/10.1016/0378-4371(92)90416-n
3. Jean, M. (1999). The non-smooth contact dynamics method. *Computer Methods in Applied Mechanics and Engineering, 177 (3-4),* 235–257. https://doi.org/10.1016/s0045-7825(98)00383-1
4. Haff, P. K., Werner, B. T. (1986). Computer simulation of the mechanical sorting of grains. *Powder Technology, 48 (3),* 239–245. https://doi.org/10.1016/0032-5910(86)80048-1
5. Kruggel-Emden, H., Simsek, E., Rickelt, S., Wirtz, S., Scherer, V. (2007). Review and extension of normal force models for the Discrete Element Method. *Powder Technology, 171 (3),* 157–173. https://doi.org/10.1016/j.powtec.2006.10.004
6. Malone, K. F., Xu, B. H. (2008). Determination of contact parameters for discrete element method simulations of granular systems. *Particuology, 6 (6),* 521–528. https://doi.org/10.1016/j.partic.2008.07.012
7. Machado, M., Moreira, P., Flores, P., Lankarani, H. M. (2012). Compliant contact force models in multibody dynamics: Evolution of the Hertz contact theory. *Mechanism and Machine Theory, 53,* 99–121. https://doi.org/10.1016/j.mechmachtheory.2012.02.010
8. Suhr, B., Six, K. (2016). Friction phenomena and their impact on the shear behaviour of granular material. *Computational Particle Mechanics, 4 (1),* 23–34. https://doi.org/10.1007/s40571-016-0119-2
9. Filippo, M., Di Felice, R. (2021). On the Influence of Contact Models on Friction Forces in Discrete Element Method Simulations. *Chemical Engineering Transactions, 86,* 811–816.
10. Man, T., Zhang, P., Ge, Z., Galindo-Torres, S. A., Hill, K. M. (2022). Friction-dependent rheology of dry granular systems. *Acta Mechanica Sinica, 39 (1).* https://doi.org/10.1007/s10409-022-22191-x
11. Luding, S., Clément, E., Blumen, A., Rajchenbach, J., Duran, J. (1994). Onset of convection in molecular dynamics simulations of grains. *Physical Review E, 50 (3),* R1762–R1765. https://doi.org/10.1103/physreve.50.r1762
12. Luding, S. (2008). Cohesive, frictional powders: contact models for tension. *Granular Matter, 10 (4),* 235–246. https://doi.org/10.1007/s10035-008-0099-x
13. Führer, F., Brendel, L., Wolf, D. E. (2024). Correction of the spring-dashpot-slider model. *Granular Matter, 26 (2).* https://doi.org/10.1007/s10035-024-01424-4
14. Mindlin (1949). *Compliance Of Elastic Bodies In Contact.* Available at: https://www.researchgate.net/profile/Valentin-Popov-2/post/Does-anyone-have-an-electronic-copy-of-1949-paper-by-Mindlin-Compliance-of-Elastic-Bodies-in-Contact-JAM-16-1949/attachment/5fcfedf53b21a2000160b8d3/AS%3A966581471440897%401607462389742/download/Mindlin_1949_ComplianceOfElasticBodiesInContact.pdf
15. Walton, O. R., Braun, R. L. (1986). Viscosity, granular-temperature, and stress calculations for shearing assemblies of inelastic, frictional disks. *Journal of Rheology, 30 (5),* 949–980. https://doi.org/10.1122/1.549893
16. Shäfer, J., Dippel, S., Wolf, D. E. (1996). Force Schemes in Simulations of Granular Materials. *Journal de Physique I, 6 (1),* 5–20. https://doi.org/10.1051/jp1:1996129
17. Heslot, F., Baumberger, T., Perrin, B., Caroli, B., Caroli, C. (1994). Creep, stick-slip, and dry-friction dynamics: Experiments and a heuristic model. *Physical Review E, 49 (6),* 4973–4988. https://doi.org/10.1103/physreve.49.4973
18. Bengisu, M. T., Akay, A. (1999). Stick–slip oscillations: Dynamics of friction and surface roughness. *The Journal of the Acoustical Society of America, 105 (1),* 194–205. https://doi.org/10.1121/1.424580
19. Togo, T., Shimamoto, T. (2012). Energy partition for grain crushing in quartz gouge during subseismic to seismic fault motion: An experimental study. *Journal of Structural Geology, 38,* 139–155. https://doi.org/10.1016/j.jsg.2011.12.014
20. Persson, B. N. J. (2013). *Sliding Friction: Physical Principles and Applications.* Springer Science & Business Media.

21. Berman, A. D., Ducker, W. A., Israelachvili, J. N. (1996). Origin and Characterization of Different Stick-Slip Friction Mechanisms. *Langmuir, 12 (19),* 4559–4563. https://doi.org/10.1021/la950896z
22. Dunham, E. M., Rice, J. R. (2008). Earthquake slip between dissimilar poroelastic materials. *Journal of Geophysical Research: Solid Earth, 113 (B9)*. https://doi.org/10.1029/2007jb005405
23. Singh, T. N., Verma, A. K., Kumar, T., Dutt, A. (2011). Influence of shear velocity on frictional characteristics of rock surface. *Journal of Earth System Science, 120 (1),* 183–191. https://doi.org/10.1007/s12040-011-0009-1
24. Yang, C.-M., Yu, W.-L., Dong, J.-J., Kuo, C.-Y., Shimamoto, T., Lee, C.-T., Togo, T., Miyamoto, Y. (2014). Initiation, movement, and run-out of the giant Tsaoling landslide – What can we learn from a simple rigid block model and a velocity-displacement dependent friction law? *Engineering Geology, 182,* 158–181. https://doi.org/10.1016/j.enggeo.2014.08.008
25. Armstrong-Hélouvry, B., Dupont, P., De Wit, C. C. (1994). A survey of models, analysis tools and compensation methods for the control of machines with friction. *Automatica, 30 (7),* 1083–1138. https://doi.org/10.1016/0005-1098(94)90209-7
26. Luding, S., Clément, E., Blumen, A., Rajchenbach, J., Duran, J. (1994). Anomalous energy dissipation in molecular-dynamics simulations of grains: The «detachment» effect. *Physical Review E, 50 (5),* 4113–4122. https://doi.org/10.1103/physreve.50.4113
27. Ketterhagen, W. R., Curtis, J. S., Wassgren, C. R. (2005). Stress results from two-dimensional granular shear flow simulations using various collision models. *Physical Review E, 71 (6)*. https://doi.org/10.1103/physreve.71.061307
28. Teufelsbauer, H., Wang, Y., Pudasaini, S. P., Borja, R. I., Wu, W. (2011). DEM simulation of impact force exerted by granular flow on rigid structures. *Acta Geotechnica, 6 (3),* 119–133. https://doi.org/10.1007/s11440-011-0140-9
29. Mansouri, M., El Youssoufi, M. S., Nicot, F. (2016). Numerical simulation of the quicksand phenomenon by a 3D coupled Discrete Element – Lattice Boltzmann hydromechanical model. *International Journal for Numerical and Analytical Methods in Geomechanics, 41 (3),* 338–358. https://doi.org/10.1002/nag.2556
30. Gallas, J. A. C., Herrmann, H. J., Sokołowski, S. (1992). Molecular dynamics simulation of powder fluidization in two dimensions. *Physica A: Statistical Mechanics and Its Applications, 189 (3-4),* 437–446. https://doi.org/10.1016/0378-4371(92)90055-u
31. Melin, S. (1994). Wave propagation in granular assemblies. *Physical Review E, 49 (3),* 2353–2361. https://doi.org/10.1103/physreve.49.2353
32. Wei, H., Li, M., Li, Y., Ge, Y., Saxén, H., Yu, Y. (2019). Discrete Element Method (DEM) and Experimental Studies of the Angle of Repose and Porosity Distribution of Pellet Pile. *Processes, 7 (9),* 561. https://doi.org/10.3390/pr7090561
33. Wei, S., Wei, H., Saxen, H., Yu, Y. (2022). Numerical Analysis of the Relationship between Friction Coefficient and Repose Angle of Blast Furnace Raw Materials by Discrete Element Method. *Materials, 15 (3),* 903. https://doi.org/10.3390/ma15030903
34. Dhaouadi, W., Marteau, E., Kolvenbach, H., Choukroun, M., Molaro, J. L., Hodyss, R., Schulson, E. M. (2021). Discrete element modeling of planetary ice analogs: mechanical behavior upon sintering. *Granular Matter, 24 (1)*. https://doi.org/10.1007/s10035-021-01167-6

✉***Abdelghani Khellaf,*** *PhD Student, Department of Civil Engineering, Ferhat Abbas University Setif 1, Setif, Algeria, e-mail: khellafabdelghani3@gmail.com, ORCID: https://orcid.org/0000-0002-7593-4954*

Mouloud Mansouri, *MCA Dr., Department of Civil Engineering, Ferhat Abbas University Setif 1, Setif, Algeria, ORCID: https://orcid.org/0000-0002-4179-7488*

✉*Corresponding author*